AIAA 80-0405R

Practical Method of Crack Growth Analyses for Fighter Aircraft

M. Levy,* A. S. Kuo,† and K. Grube†
Fairchild Republic Company, Farmingdale, N. Y.

The relationship between crack growth rate under variable amplitude spectrum da/dF and the stress intensity factor per unit stress α is found to be unique for similar loading spectra. Once this relationship, $f(\alpha)$, is established, the cycle-by-cycle integration is not needed and simple integration of $f(\alpha)$ can be applied to obtain the crack growth curve. An illustration of the da/dF vs α approach as recommended for the A-10A Damage Tolerance Reassessment is demonstrated. It includes two different stress spectra applied on coupon tests with various geometry and loading configurations. The function $f(\alpha)$ assumes the form used by the Forman equation for da/dN, normalized about some reference stress. This function is shown to fit best the data points generated by the coupon test.

Nomenclature

A	= effective crack length
a	= crack length measured on the surface at the edge of a hole
da/dF	= crack growth rate for randomized flight-by-flight spectrum
da/dN	= constant amplitude crack growth rate
c	= crack length measured along edge of a hole
c°	= fraction of load transfer
D	= hole diameter
F	= 1 life of randomized spectrum A-10A
K	= stress intensity factor
ΔK	= stress intensity factor range
R	= stress ratio
s	= stress level ratio
t	= thickness
W	= width
W_p	= effective width for load transfer
α	= stress intensity factor per unit stress
σ	= stress
$\bar{\sigma}$	= root mean square of stresses in a spectrum

Superscripts and Subscripts

c	= critical
eff	= effective
f	= final
max	= maximum
min	= minimum
o	= initial

Introduction

SINCE the evaluation by the U.S. Air Force of the design philosophy that cracks are assumed to be initially present in all airframe Safety of Flight Structure,‡ the objective of accurately predicting crack growth in these structures without incurring the penalties of costly and time-consuming computer usage has become of particular importance. For typical damage tolerance design[1] and assessment in fighter-type aircraft, many fracture critical areas have to be examined. Simplification of the analysis procedures which can readily be verified by coupon testing is a key ingredient to accurately and more economically performing the damage tolerance design and assessment task. In an expansion of the existing fatigue crack growth prediction concepts,[2-6] this paper proposes a correlation between the slope of the crack growth vs flight curve da/dF, which is reduced from coupon test data, and the stress intensity factor per unit stress α. This correlation is closely bounded for 2024-T3 type aluminum alloys subject to given random fighter-type flight-by-flight stress spectra. An experimental relationship was established and used to show how an analytic retardation model might be selected and verified. The important follow-on result, however, is that a single relationship can be used for crack growth predictions in

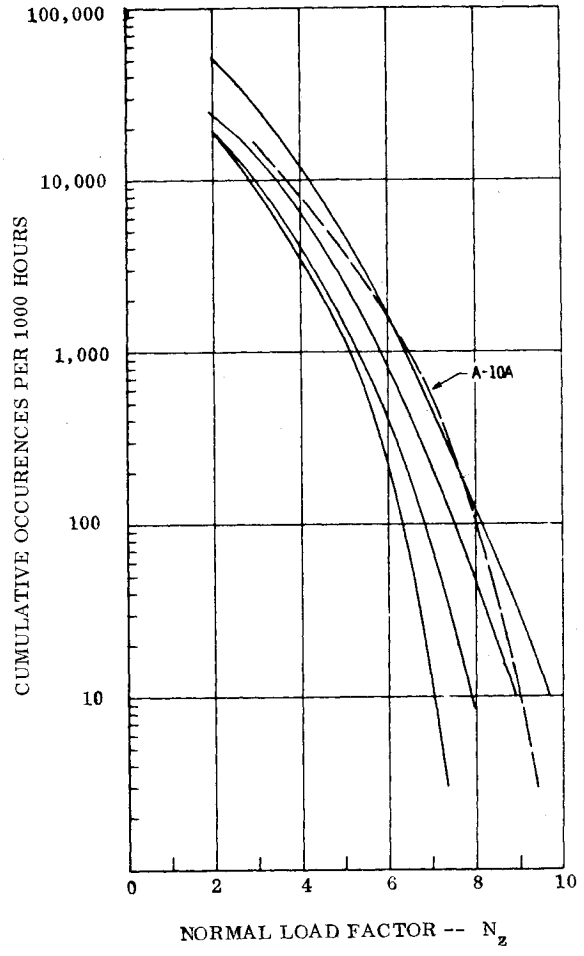

Fig. 1 Typical fighter aircraft exceedances presently in service.

Submitted Jan. 10, 1980; presented as Paper 80-0405 at the AIAA 18th Aerospace Sciences Meeting, Pasadena, Calif., Jan. 14-16, 1980; revision received June 23, 1980.

*System Design Engineer.

†Senior System Design Engineer.

‡Safety of Flight Structure is defined in MIL-A-83444 as a structure whose failure could cause direct loss of an aircraft or whose failure, if remaining undetected, could result in the loss of an aircraft.

typical aircraft structural geometries subjected to random fighter-type similar stress spectra characterized by various related stress levels.

The first part of the paper presents the details on the stress spectra and the coupon tests. In the second part, the development of the crack growth equations, the consolidation of all the experimental data, and the description of the data after consolidation by the governing equations are presented. Lastly, the relationship to the analytic approach of crack growth prediction with retardation and one example of the use of the results for life prediction of a typical structure encountered in fighter aircraft design are given.

Spectrum

The flight-by-flight spectrum used in this study was the 262,000 cycles/lifetime A-10A composite maneuver spectrum.[7] This spectrum is one of the more severe fighter aircraft spectra flown today, as shown in Fig. 1. The generation of the flight-by-flight sequence used in test was accomplished by means of a random number generator computer routine operated against the 205 unique maneuver conditions in the A-10A spectrum in a descending aircraft gross weight pattern. A mission mix of 11 separate missions formed the composite. A representative sequence of ground maneuver conditions is interspersed between flights in the random flight-by-flight sequence used in test. The resulting flight-by-flight random sequence is a repeatable segment equal to 4% of one lifetime. Occurrences of maneuver conditions not repeatable in each 4% random sequence are randomly distributed within each flight to achieve the correct amount of occurrences per lifetime of these conditions. Approximately 3000 flights make up one lifetime or 6000 h of flight. Stress spectra representative of the inboard lower wing cover of the A-10A aircraft were calculated for each unique spectrum condition using reference stress levels of 39.28 and 35.1 ksi as the maximum spectrum stresses.

Tests

Test specimens were manufactured from shot-peened 2024-T3511 extrusion material which was nominally 0.250 in. thick. Several specimen configurations were tested. These consisted of low ($\approx 15\%$) load transfer and no load transfer (filled or open hole) specimens. Load transfer specimens were manufactured within hole tolerance specifications which permit a range of pin fit from slight clearance (0.0015 in. on the diameter) to slight interference (0.0035 in. on the diameter). Typical specimen geometry is shown in Fig. 2.

Crack length measurements were made visually on all specimens using a 30X microscope. Tests were conducted in hydraulic load frames operated through a closed-loop computer-directed control and supervising system. The applied loads were maintained within $\pm 1\%$ of the required values.

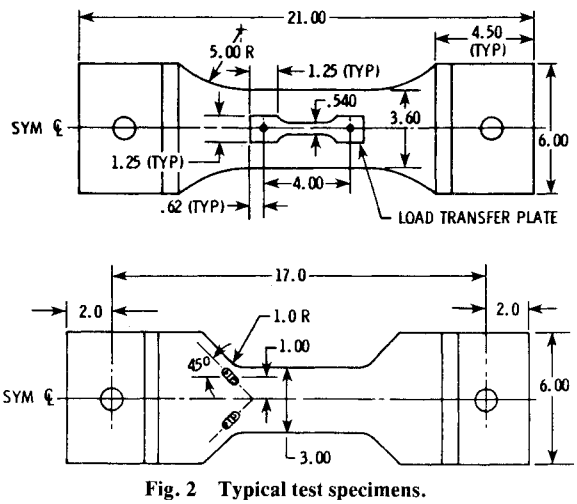

Fig. 2 Typical test specimens.

Each specimen was precracked initially to ideally produce a quarter circular corner flaw at the edge of a hole in the test section. Precracking consisted of the introduction of a 45 deg notch through electrical discharge (elox) in an initial hole smaller than the final required size hole. Cycling at constant amplitude made this flaw grow into a sharpened fatigue crack of the size desired after the initial hole was reamed to final size. In many cases however, the actual resulting flaw tended to be elliptic in cross-sectional shape. For those cases, the actual initial flaw size and shape was accounted for by using the appropriate stress intensity solution given in the Appendix. The observed crack growth behavior is presented as surface crack length vs fraction of life expended. Determination of corner crack shape during the interim period prior to breakthrough was obtained from fractographic examination of the specimen fracture surface.

A Crack Growth Prediction Method

The progress of fatigue and fracture research has made it possible to predict fatigue crack growth more accurately than ever before. A great advance is the utilization of the stress intensity factor K to characterize fatigue crack growth shown by Paris.[2] Fatigue crack growth rate can be uniquely related to K, because K is able to represent the combined effect of geometry and load on the crack tip deformation. Therefore, coupon testing data can be used directly to predict crack growth in actual structures using a cycle-by-cycle integration method. This approach has been shown to be very successful for simple cases of constant amplitude fatigue loading.

In actual aircraft service conditions, loads are far from being constant. Hence, variable amplitude flight-by-flight randomized spectra are now typically used to simulate actual service loads. In the prediction of crack growth under variable amplitude load spectra, the results are often found to be too conservative if load interaction is not properly treated. Willenborg,[8] Wheeler,[9] and closure models[10] are the popular approaches to treat the crack growth retardation behavior due to the overload effect. These models have shown various degrees of success. However, in order to have full confidence in predictions using these techniques, experimental verification and/or adjustment is required.

The cycle-by-cycle integration method is the basic way of predicting crack growth under any kind of load spectrum. If analyses are needed for several critical fracture locations subjected to the same or similar load spectrum, the cycle-by-cycle integration method becomes costly. A recent suggestion for crack growth prediction for aircraft is to use da/dF (crack growth per flight) instead of da/dN (crack growth per cycle).[6,11,12] In the da/dF approach, the cycle-by-cycle integration method is, again, needed to obtain da/dF for a specific stress spectrum. The resulting da/dF can then be used to predict crack growth of other locations subjected to the same stress spectrum without resorting to the integration of crack growth through all of the load-cycles in the given spectrum. Substantial computer CPU time, however, can be saved with the da/dF approach when da/dF is developed directly from experimental crack growth test data. In addition, this will provide an avenue to assess various spectra of related stress levels.

Paris[2] suggested that da/dN of variable amplitude random load spectra can be characterized by $\bar{K}_{max} = \bar{\sigma}_{max}\alpha$. The theoretical and analytical works of Smith,[3] Swanson et al.,[4] and Barsom[5] support Paris' suggestion. Paris' approach was applied to da/dF by Gallagher[11] who, in the light of the works of Paris[2] and Forman et al.,[13] proposed the following equation form for correlation da/dF vs $\bar{K}_{max}$ data,

$$\frac{da}{dF} = \frac{C\bar{K}^m_{max}}{K_c - \bar{K}_{max}} \tag{1}$$

where K_c is fracture toughness, C and m are empirical constants to be determined from a best data fitting process. Schijve[14] also pointed out that da/dF vs $\bar{K}_{max}$ approach could be applicable to similar spectra. According to Eq. (1), experimental data points of da/dF vs $\bar{K}_{max}$ for similar spectra should fall into a line. Gallagher and Stalnaker's[11] test data for bomber-type spectra with three different stress levels indicate good correlation between da/dF and $\bar{K}_{max}$. The bomber-type spectrum, however, is relatively mild in comparison with a typical fighter spectrum. In a bomber-type spectrum the load interaction is considerably less severe than in the fighter spectrum, making the burden of proof for da/dF vs $\bar{K}_{max}$ for fighter spectra fall on new test substantiation.

Since the characteristic stress intensity factor $\bar{K}_{max}$ is defined as $\bar{K}_{max}=\bar{\sigma}_{max}\alpha$, a natural alternative to da/dF vs $\bar{K}_{max}$ is da/dF vs α. Brussat[15] has used $\alpha=K/\sigma$ to characterize variable amplitude crack growth. The use of α would circumvent the need to justify $\bar{\sigma}_{max}$ as a characteristic stress for a spectrum. As a matter of fact, $\bar{\sigma}_{max}$ is a constant for a specific spectrum and hence there is no need to consider it at all. For similar spectra, two approaches are proposed in this paper to account for the differences in stress levels among each individual similar spectrum. The stress level ratio s which is defined as the ratio of the maximum peak stress in a less severe stress spectrum to the maximum peak stress in the most severe or baseline reference stress spectrum, is an index to represent the severities among similar spectra. The word "similar" in this context means that there exists, roughly, a one-to-one correspondence in each stress cycle for each similar spectrum and the magnitude of each stress cycle in a spectrum can be scaled from that of the reference spectrum, which is usually chosen to be the severest spectrum.

One approach to account for stress level of a spectrum is to use effective stress intensity factor coefficient $\bar{\alpha}$ which is defined as $\bar{\alpha}=s\alpha$. The da/dF is then characterized in terms of $\bar{\alpha}$ instead of α. A plot of experimental da/dF vs $\bar{\alpha}$ data points from spectra with different stress levels should fall into a narrow band. The following form of equation is proposed for da/dF vs $\bar{\alpha}$ correlation,

$$\frac{da}{dF}=\frac{C\bar{\alpha}^m}{\alpha_c-\bar{\alpha}} \tag{2}$$

where α_c, C, and m are empirical constants to be determined from a best data fitting procedure. It should be noted that α_c for a group of similar spectra is not a purely empirical constant although it is determined from a data fitting procedure. The magnitude of α_c depends, to a great extent, on the K_c value of the material under investigation. The meaning of α_c is in parallel to that of K_c.

The other approach to account for stress level of a spectrum in proposed in the following equation,

$$\frac{da}{dF}=\frac{C\alpha^m}{(\alpha_c/s)-\alpha}s^n \tag{3}$$

If n is equal to $m-1$, Eq. (3) is identical to Eq. (2). α_c, C, m, and n are empirical constants to be determined by best data fitting procedure. The implication of Eq. (3) is that if $(da/dF)/s^n$ is plotted against α for spectra with different s then the test data will fall into a narrow band. Although the implementation of Eq. (3) would require more effort, it does offer more freedom via the constant n to find an equation which best fits the test data.

The two approaches described in the last two paragraphs for the characterization of experimental da/dF shall be verified in later sections of this paper. While they appear slightly different in form, both Eqs. (2) and (3) are, in essence, based upon the same concept that da/dF can be uniquely related to α.

With the empirical da/dF vs α relation available, the crack growth integration method briefly outlined below can be used to obtain the damage tolerance life interval ΔF_i for extending a crack from a_{i-1} to a_i. Rewrite Eq. (2) or (3) as follows,

$$\frac{da}{dF}=f(\alpha) \tag{4}$$

then $dF=da/f(\alpha)$

$$\Delta F_i=\int_{a_{i-1}}^{a_i}\frac{da}{f(\alpha)},\quad i=1,2,\ldots N \tag{5}$$

Since α can hardly be expressed in explicit form as a function of a for actual aircraft structures, Eq. (5) cannot be integrated to obtain closed-form solutions. Numerical integration methods, e.g., trapezoidal or Simpson's rule, are usually used to evaluate Eq. (5). The accumulated damage tolerance life F_i required to extend crack from a_o to a_i is:

$$F_i=\sum_{j=1}^{i}\Delta F_j \tag{6}$$

The thus calculated pairs of points, i.e., a_i vs F_i, are used to construct fatigue crack growth vs life curve. It is obvious that the numerical integration of Eq. (5) would need much less CPU time than the cycle-by-cycle integration method.

The proposed experimental da/dF vs α correlation is a reliable and economical approach to predict fatigue crack growth under similar spectra, which will insure the safety and durability of fleet aircraft. It is recognized that load interaction often handicaps an accurate theoretical prediction of crack growth under variable amplitude stress spectrum. Broek and Smith[12] reported that a wide range of life to reach the same crack length was obtained using different load-interaction models such as Willenborg, Wheeler, and closure models. In order to make reliable predictions, any load-interaction model would need adjustments according to experimental data. In this way, the sum of the costs due to analytical and experimental work will be enormous. A practical approach would be using the experimentally determined da/dF vs α data as the base of analysis. The use of experimental da/dF would avoid the analytical difficulties with load interaction. The use of da/dF instead of cycle-by-cycle integration would substantially simplify analysis and reduce CPU time in analyzing a group of fracture critical locations subjected to similar spectra. Test data of da/dF for three stress levels would likely be sufficient to establish a generalized da/dF vs α data base such as Eqs. (2) and (3) for structures subjected to similar spectra.

Experimental Results and Discussions

The raw test data are plotted in Fig. 3 as curves of surface crack length vs fraction of crack growth life. Table 1 shows the flaw sizes and their corresponding growth at successive stages of testing for each individual specimen. Since the initial surface crack length is different for each specimen, the curves in Fig. 3 were plotted from 0.05 in. surface crack length or greater to facilitate a relative comparison. Figure 3 shows that for the same high stress level, high pin load transfer results in a much shorter life than low pin load transfer. Figure 3 also shows that for the same intermediate stress level, open hole specimens of 0.5 in. diameter exhibit much shorter life than the low pin load transfer specimens of 0.25 in. diameter hole.

Figure 4 is a 5X photograph of the fracture surface of a typical test specimen. The photograph indicates that the flaw shape is elliptical before breakthrough and is becoming quarter circular during the transition to breakthrough. Table 1 shows typically that the major part of fatigue life was spent in the period from initial flaw to breakthrough. Therefore, it

Table 1 Life vs crack length measurements

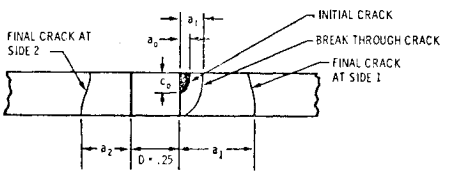

Test S/N	Loading condition: Max stress, ksi	Max load transfer, %	Life at break-through, h	Life at second crack initiation, h	Life at failure, h	Initial crack: a_o, in.	Initial crack: c_o, in.	Break-through a_f, in.	Final crack: a_1, in.	Final crack: a_2, in.	Aspect ratio: a_o/c_o	Aspect ratio: a_f/t
0-4/7	39.28	5.0	0[a]	480	1,943	0.118	Thru	0.118	0.580	0.380	Thru	0.472
0-4/8	39.28	5.0	0[a]	6240	6,888	0.056	Thru	0.056	0.625	0.250	Thru	0.224
0-4/13	39.28	5.0	7920	9360	10,102	0.018	0.086	0.136	0.390	0.170	0.209	0.618
0-4/14	39.28	5.0	5520	7440	7,718	0.027	0.089	0.184	0.440	0.160	0.303	0.836
0-10/3	39.28	15.0	1440	1680	3,126	0.031	0.080	0.109	0.250	0.240	0.388	0.436
0-10/4	39.28	15.0	1680	2160	3,294	0.023	0.078	0.115	0.320	0.290	0.295	0.460
1-10/1	39.28	0.0(csk)	120	Unknown	2,397	0.107	0.189	0.225	0.560	0.105	0.566	0.750
1-10/2	39.28	0.0(csk)	240	None	1,442	0.170	0.275	0.194	0.620	None	0.618	0.647
2-5/7	39.28	15.0	4800	5040	6,787	0.020	0.079	0.083	0.350	0.290	0.253	0.332
0-12/3[b]	35.10	Open hole	3180	None	5,340	0.040	0.125	0.170	0.582	None	0.320	0.566
0-12/4[b]	35.10	Open hole	1800	None	3,360	0.065	0.180	0.145	0.514	None	0.361	0.483
0-5/9[c]	35.10	5.0	–	None	15,120	0.028	0.088	–	0.175	None	0.318	–

[a] Through the thickness flaw. [b] $D = 0.50$ in. [c] No break through the thickness or failure, test stopped at 15,120 h.

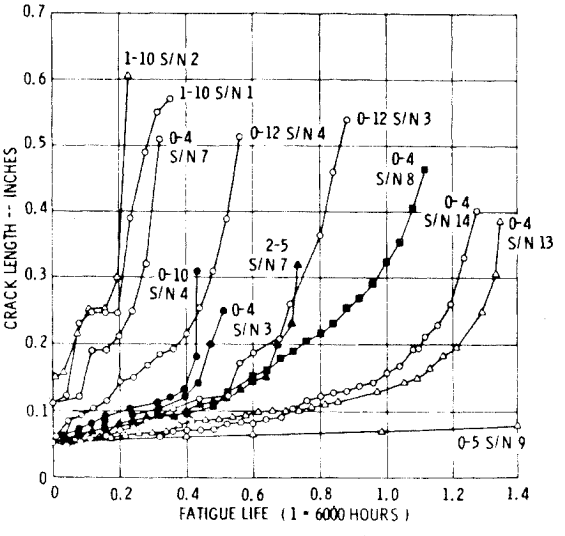

Fig. 3 Crack growth data.

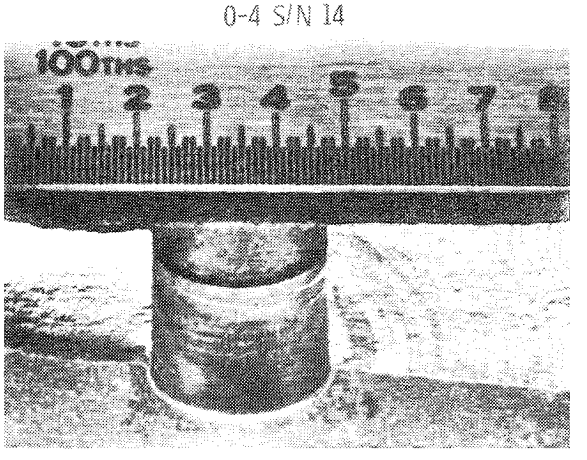

Fig. 4 Fracture surface of typical test specimen.

is important to account for flaw shape in calculating stress intensity factor; it is in contrast to the conventional practice of treating a corner flaw as quarter circular. This point is particularly important to the relatively thick sections typically found in airframe structures. Although the test specimens exhibit the beach mark appearance which is associated with fatigue crack growth, the marks can hardly by identified with either the number of 4% life blocks (see section on Spectrum) used in testing or the severest stress cycles in a 4% life block. This is attributed to the randomness of the test spectrum along with the ductility properties of 2024 aluminum alloys. Recent advances,[16] however, have shown that a low-high sequence of cyclic loading of short duration interspersed at regular intervals will provide unique growth markings in the fracture surfaces of 2024 aluminum alloy when subjected to random flight-by-flight cyclic loadings. This approach has been successfully used in a later group of test specimens.

The test data shown in Fig. 3 was evaluated using seven points incremental polynomial method to obtain da/dF vs a data. This method is recommended by ASTM[17] to process da/dN data. The stress intensity factor per unit stress α for a given flaw configuration was calculated with the method described in the Appendix. The resulting da/dF vs a and α vs a data were then used to establish da/dF vs α data for each specimen. Next, the da/dF vs α data were characterized in terms of the two proposed methods mentioned in the last section to account for the spectrum stress levels.

Figure 5 shows a composite of all data points plotted as da/dF vs $s\alpha$. The method of least squares was used to evaluate the unknown constants of Eq. (2) and is shown as Eq. (7):

$$\frac{da}{dF} = \frac{0.3785(s\alpha)^{4.735}}{1.4 - s\alpha} \tag{7}$$

The coefficient of correlation and modified standard error are 0.9387 and 0.1708, respectively. Figure 5 also shows a solid line representing Eq. (7) and two dashed lines representing one standard deviation from Eq. (7). Figure 5 clearly shows that all data points fall into a narrow band characterized by plus and minus one standard deviation regardless of geometric factors and stress levels. This relationship appears to corroborate the scatter exhibited by raw da/dN data for 2024 aluminum alloy. For the same α, it is obvious that the

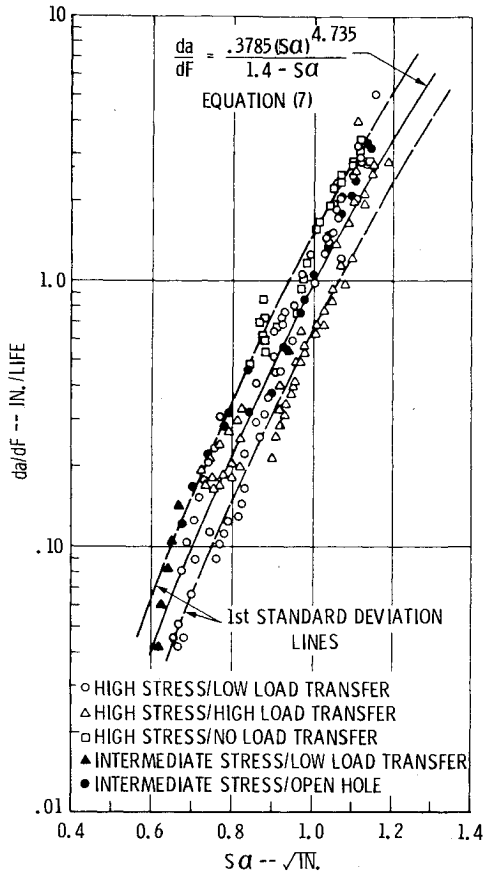

Fig. 5 da/dF vs $s\alpha$ test data and best fit curve.

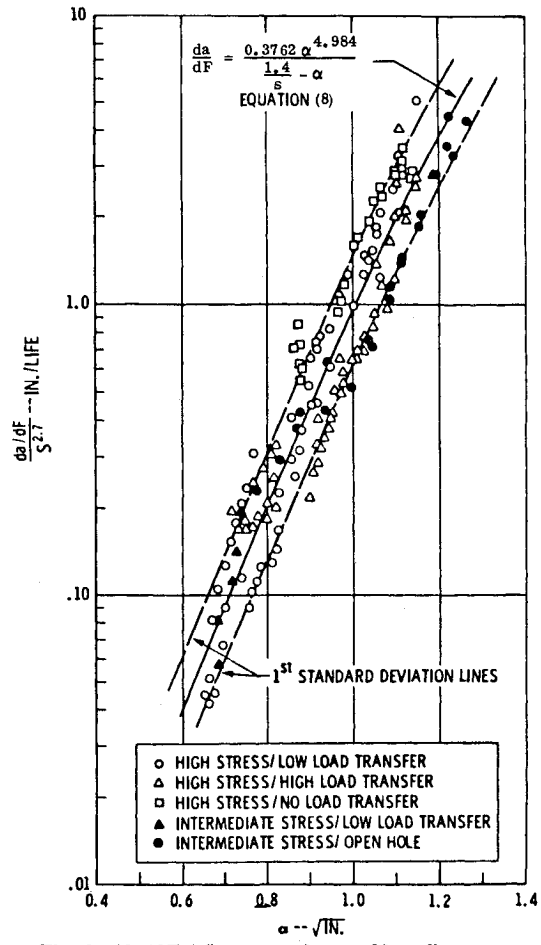

Fig. 6 $(da/dF)/s^n$ vs α test data and best fit curve.

da/dF from the spectrum of high stress level ($s=1.0$) are higher than the da/dF from the spectrum of intermediate stress level ($s=0.893$). The implication of Fig. 5 is that at the same $s\alpha$, da/dF would be the same for all similar spectra regardless of stress levels.

Figure 6 shows a composite of all data points plotted as $(da/dF)/s^n$ vs α. The da/dF vs α data from tests with the higher stress level were first used to evaluate constants C and m in Eq. (3); then this relationship was compared with the test data from the lower stress level to find the constant n. The method of least squares was used to establish the best fitting curve. Equation (3) with all constants evaluated is shown as Eq. (8):

$$\frac{da}{dF} = \frac{0.3762\alpha^{4.984}}{(1.4/s)-\alpha} s^{2.7} \tag{8}$$

The coefficient of correlation and modified standard error based upon the data points from tests with the higher stress level ratio for Eq. (8) are 0.9348 and 0.176, respectively. Figure 6 also shows a solid line representing Eq. (8) and two dashed lines representing plus and minus one standard deviation. The figure clearly shows that all data points fall into a narrow band defined by plus and minus one standard deviation lines in spite of differences in geometric factor and stress level. The implication of Fig. 6 is that at the same α, $(da/dF)/s^n$ obtained from similar spectra of different stress level ratio would be the same.

The aforementioned coefficients of correlation and modified standard errors are statistical quantities to measure the degree of correlation and fit between test data and Eqs. (7) and (8), respectively. The slight differences among these numbers indicate that either Eq. (7) or (8) can be closely fit to test data. However, to demonstrate the flexibility of Eq. (3), a plot of Eqs. (7) and (8) together with test data from tests with $s=0.893$ only is shown in Fig. 7. Comparing Eqs. (7) and (8) with respect to the data points of Fig. 7 indicates that Eq. (8) provides a better fit. This result shows the value of evaluating the constant n in Eq. (8) for improved analysis precision.

It should be emphasized that the experimental da/dF data of this investigation were collected under a variety of initial flaw configurations, loading conditions, and specimen geometries. Therefore, Figs. 5 and 6 together with Eqs. (7) and (8) sufficiently demonstrate that experimental da/dF can be uniquely characterized with the stress intensity factor per unit stress α. Equations (7) and (8) will be the bases for crack growth analysis in an example to be described later.

Figures 5-7 can serve as baseline data for verifying and/or adjusting any theoretical load-interaction models. Since the crack length at various stages of life is obtained by an integration of $da/dF=f(\alpha)$ relation, any theoretical prediction method should yield a $f(\alpha)$ which falls onto a band defined by tested da/dF vs α data. Any deviation from test data would necessitate adjustments of the candidate theoretical load-interaction model. It has been reported that different Wheeler constants were needed for a reasonable fit between test and theoretical crack growth vs life curve even though specimens of different geometry were made of the same material and were tested under similar or same load spectra.[12,18] A common practice of dealing with this problem is to use an average Wheeler constant as a compromise among specimens. An alternative is suggested in Figs. 5 and 6: that the appropriate Wheeler constant should be selected such that the resulting da/dF would fall onto tested da/dF. In this manner, one could have a direct quantitative feeling of the compromise among specimens for the Wheeler constant selected.

Two theoretical curves predicted by the cycle-by-cycle integration method using the Willenborg and Wheeler models are shown in Fig. 8. The Willenborg model falls on the upper

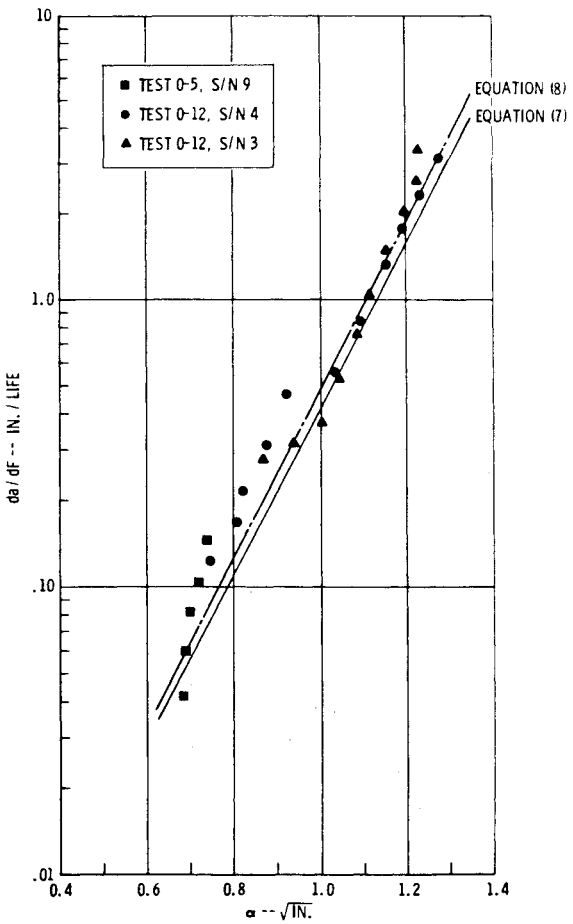

Fig. 7 da/dF vs α for intermediate stress level.

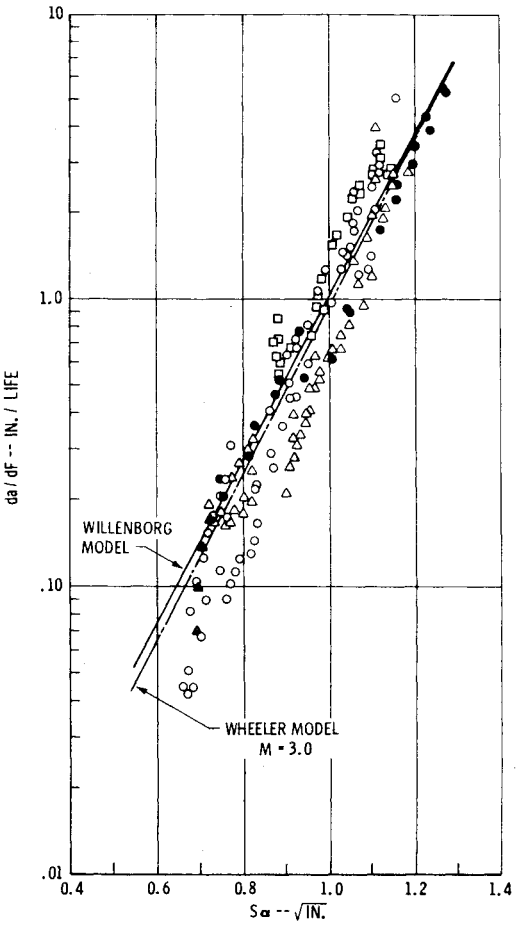

Fig. 8 Cycle-by-cycle theoretical models vs test data.

bound of test data, and it leads to a conservative prediction. The Wheeler model falls reasonably well within the test data when the Wheeler constant is 3.0. It is noted that either Willenborg or Wheeler model predicts higher da/dF in the low α region which occupies the major portion of life (see Fig. 8). The Willenborg model can hardly be adjusted to conform with test data except through the change of baseline da/dN material properties, which must be statistically demonstrated. In trying different Wheeler constants for best fit to test data, it was observed that the predicted curves corresponding to different Wheeler constants are approximately parallel to one another. Consequently, if this group of curves is not parallel to the band defined by test data, no single Wheeler constant can be selected such that the predicted Wheeler curve will follow the shape of test band for the whole range of α under investigation. The agreement between predicted and test crack growth vs life curve is often the result of a fortuitous balance between the overestimation and underestimation of da/dF in the low α and high α regions, respectively. In general the validation of analytic load interaction retardation models by the da/dF method is a complicated process often involving the use of trial and error. It can also be seen that, in the case of the Wheeler model, the actual constant becomes a variable over the range of α.

Example

All illustration of how the da/dF vs α concept is used in predicting life is described in this section. The specimen in Fig. 2b is designed to represent one of the fracture critical areas in the wing lower skin of the A-10A aircraft. Due to the rapid change in cross-sectional area and the proximity of the plate nut location with respect to the edge of the plate, there is a local stress rise of approximately 60% at this section. The initial flaw was introduced by the same method described in the section on Tests and was located at the plate nut hole, $D=0.1$ in., closest to the edge of the plate. The previously described randomized flight-by-flight spectrum was applied, and crack measurements were made on both sides of the hole every 240 h of spectrum testing. The specimen failed at 2300 h (see Fig. 9). The fracture surface was examined under a microscope to verify initial, breakthrough, and final crack lengths. The analytical prediction was done by using the empirical data shown in Figs. 6 and 7. Equation 7 was integrated using Simpson's rule:

$$\frac{da}{dF} = \frac{0.3785\alpha^{4.735}}{1.4-\alpha}$$

$$\Delta F_i = \int_{a_{i-1}}^{a_i} \frac{1.4-\alpha}{0.3785\alpha^{4.735}}\, da,\ i=1, 2,\ldots N \tag{9}$$

The relationship between a and α was generated according to the Appendix for use in the integration of Eq. (9).

The Willenborg and Wheeler models were applied using the cycle-by-cycle integration method and da/dN data in the form of Forman's equation,

$$\frac{da}{dN} = \frac{0.784\times 10^{-8}\Delta K^{4.036}}{(1-R)83-\Delta K} \tag{10}$$

The Forman's constant shown in Eq. (10) were obtained from da/dN data for 2024-T3 plate material.[19] The theoretical models showed less life than the actual test, while the empirical data were accurate in predicting crack growth life. The accuracy of the analytic analysis methods is highly dependent on material da/dN data. The point that must be emphasized is the accuracy of predicting life and the cost in terms of

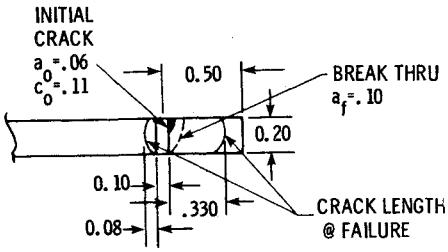

Crack Geometries for Illustrated Problem

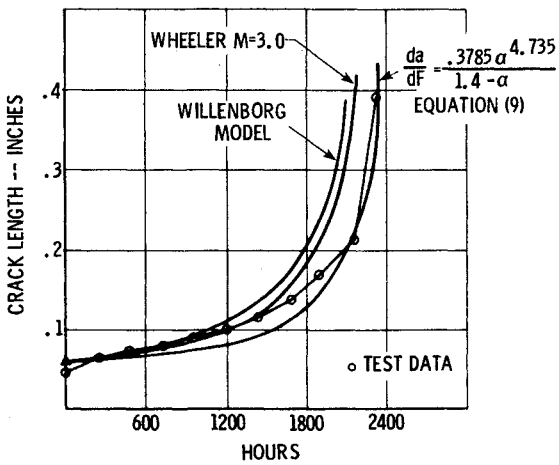

Fig. 9 Illustration of theoretical models vs da/dF scheme in predicting crack growth.

computer CPU time in generating crack growth data which is approximately 15:1 in favor of da/dF vs α type integration.

Conclusions

The following conclusions are offered based on the analysis of the test results presented herein:

1) da/dF vs α data collected from tests under various specimen geometry and similar fighter-type stress spectra fall into a narrow band. This fact suggests that da/dF can be characterized by a single parameter α.

2) The differences in stress level among similar spectra can be solved by either replacing α with $s\alpha$ or modifying da/dF with a factor $1/s^n$.

3) The application of experimental da/dF vs α relationship for analyzing crack growth life is a reliable and economic way to fulfill the aircraft damage tolerance design and assessment task.

4) The experimental da/dF vs α relationship can be used to verify and adjust analytical load-interaction models.

Appendix

The stress intensity factor (SIF) for an elliptical corner flaw at the edge of a hole is known to vary along the crack front. The majority of specimen tests used in development of this paper show change in the aspect ratio of the crack. To account for this change, actual initial and breakthrough crack aspect ratio are considered. The crack shape between the two intervals is assumed to change proportionally. The expression for SIF used in this analysis accounts for the change in shape. Basically, it has the form of an embedded elliptical flaw with the appropriate geometric and loading corrections. Hence $\alpha = K/\sigma$ will have the following expression:

$$\alpha_{\text{corner}} = \sqrt{\pi a}(\lambda)\ (\beta)\ (f_B)\ (\gamma) \tag{A1}$$

where

$$\lambda = \frac{1.12}{\Phi}\left(\sin^2\phi + (a/c)^2\cos^2\phi\right)^{1/4} \tag{A2}$$

The expression in the parentheses is evaluated at two locations along the crack front. A weighted average is then used to approximate a single value of SIF which is assumed representative for the crack front.

Φ is an elliptical integral of the second kind and is well defined in the literature to be:

$$\Phi = \int_0^{\pi/2}\left(1 - \frac{c^2 - a^2}{c^2}\sin^2\phi\right)^{1/2} d\phi \tag{A3}$$

where

β = is the finite width correction for symmetrical and unsymmetrical crack[20]

f_B = the Bowie solutions for one or two unsymmetrical cracks[21]

γ = the load transfer correction obtained from superposition of the tension load and pin load solutions:

$$\gamma = (1 - 0.5c^\circ) + \frac{c^\circ W_p}{2\pi A}\sqrt{\frac{2A}{(D/2)+a} - 1} \tag{A4}$$

where

$$A = \frac{D}{2} + a, \qquad \text{two cracks at the edge of a hole}$$

$$A = \frac{D}{2} + \frac{a}{2}, \qquad \text{one crack at the edge of a hole}$$

To account for the transition from a corner crack to through the thickness crack the following empirical formula suggested by Ref. 22 was used,

$$\alpha_{\substack{\text{corner}\\\text{final}}} = \frac{\alpha_{\text{corner}}}{2(c/t)^2 + 1} + \frac{2(c/t)^2}{2(c/t)^2 + 1}\alpha_{\text{thru}} \tag{A5}$$

where

$$\alpha_{\text{thru}} = \sqrt{\pi a}\ (f_B)\ (\beta)\ (\gamma) \tag{A6}$$

References

[1] USAF Military Specification, MIL-A-83444, 1974.

[2] Paris, P.C., "The Fracture Mechanics Approach to Fatigue," *Fatigue—An Inderdisciplinary Approach, Proceedings of the 10th Sagamore Army Materials Research Conference,* J. J. Burke, N.L. Reed and V. Weiss, eds. Syracuse University Press, Syracuse, N.Y., 1964, pp. 107-132.

[3] Smith, S.H., "Fatigue Crack Growth under Axial Narrow and Broad Band Random Loading," *Acoustic Fatigue in Aerospace Structures,* W.J. Trapp and D.M. Forney, Jr., eds., Syracuse University Press, Syracuse, N.Y., 1965, pp. 331-360.

[4] Swanson, S.R., Cicci, F., and Hoppe, W., "Crack Propagation in Clad 7079-T6 Aluminum Alloy Sheet Under Constant and Random Amplitude Fatigue Loading," *Fatigue Crack Propagation,* ASTM STP 415, 1967, pp. 312-362.

[5] Barsom, J.M., "Fatigue-Crack Growth Under Variable Amplitude Loading in ASTM A 514B Steel," *Progress in Flaw Growth and Fracture Toughness Testing,* ASTM STP 536, pp. 147-167.

[6] Gallagher, J.P., "Estimating Fatigue Crack Lives for Aircraft: Techniques," *Experimental Mechanics,* Vol. 16, Nov. 1976, pp. 425-433.

[7] Grube, K., "Development of Flight by Flight Spectra for A-10A PDV Tests," Rev. C, Fairchild Republic Co., Report FRC SA160R9403, May 14, 1979.

[8] Willenborg, J., Engle, R.M., and Wood., H.A., "A Crack Growth Retardation Model Using an Effective Stress Concept," AFFDL Report TM-71-1-FBR, Jan. 1971.

[9] Wheeler, O.E., "Spectrum Loading and Crack Growth," *Transactions of ASME, Journal of Basic Engineering,* Jan. 1972.

[10] Elber, W., "The Significance of Crack Closure," *Damage Tolerance in Aircraft Structures,* ASTM STP 486, 1971, p. 230.

[11] Gallagher, J.P. and Stalnaker, H.D., "Developing Normalized Crack Growth Curves for Tracking Damage in Aircraft," *Journal of Aircraft,* Vol. 15, Feb. 1978, pp. 114-120.

[12] Broek, D. and Smith, S. H., "The Prediction of Fatigue Crack Growth Under Flight-by-Flight Loading," *Engineering Fracture Mechanics,* Vol. 11, 1979, pp. 123-141.

[13] Forman, R.G., Kearney, V.E., and Engle, R.M., "Numerical Analysis of Crack Propagation in Cyclic-Loaded Structures," *Transactions of ASME, Journal of Basic Engineering,* Sept. 1967.

[14] Schijve, J., "Fatigue Crack Growth Under Variable-Amplitude Loading," *Engineering Fracture Mechanics,* Vol. 11, 1979, pp. 207-221.

[15] Brussat, T.R., "Rapid Calculation of Fatigue Crack Growth by Integration," *Fracture Toughness and Slow-Stable Cracking,* ASTM STP 559, 1974, pp. 298-311.

[16] Diming, W., "Marker Band Evaluation, Analysis and Result," Fairchild Republic Co., Report FRC SA160R9416, March 15, 1979.

[17] *Annual Book of ASTM Standards,* Part 10, ASTM, Philadelphia, pp. 662-680.

[18] Parker, G.S., "Generalized Procedures for Tracking Crack Growth in Fighter Aircraft," AFFDL-TR-76-133, Jan. 1977.

[19] *Damage Tolerance Design Handbook,* Metals and Ceramics Information Center, Battelle Columbus Laboratories, Jan. 1975.

[20] Isida, M., "Stress Intensity Factors for the Tension of an Eccentrically Cracked Strip," *Transactions of ASME, Journal of Applied Mechanics,* Sept. 1966, pp. 674-675.

[21] Tweed, J. and Rooke, D.P., "The Elastic Problem for an Infinite Solid Containing a Circular Hole with a Pair of Radial Edge Cracks of Different Lengths," *International Journal of Engineering Science,* Vol. 14, 1976, pp. 925-933.

[22] Brussat, T.R. and Chiu, S.T., "Flaw Growth in Complex Structure," LR 28, Vol. I, June 10, 1977.